
Proceedings Paper:
Romo Rivera, E., Boyle, J.H., Chakrabarty, S. et al. (2025) The Role of Passive Mechanics in Asymmetrically Actuated Bioinspired Joints. In: Biomimetic and Biohybrid Systems. 14th International Conference, Living Machines 2025, 15-18 Jul 2025, Sheffield, UK. Lecture Notes in Computer Science, 15582. Springer Nature. ISSN: 0302-9743. EISSN: 1611-3349.

https://doi.org/10.1007/978-3-032-07448-5_7

The Role of Passive Mechanics in Asymmetrically Actuated Bioinspired Joints

Erick Romo Rivera[1(✉)], Jordan H. Boyle[2], Samit Chakrabarty[3], and Netta Cohen[1]

[1] School of Computer Science, University of Leeds, Leeds, UK
mnerr@leeds.ac.uk
[2] Faculty of Industrial Design Engineering, Delft University of Technology, Delft, The Netherlands
[3] School of Biomedical Sciences, University of Leeds, Leeds, UK

Abstract. Animal motor control relies on antagonistic muscle pairs. In many jointed animals, muscles are often asymmetrically sized, with one optimised for maximal force generation and its counterpart tuned for fine control and stability. This inherent asymmetry, combined with passive structures of the joint, integrates dexterity and power in a directionally biased manner. While conventional robotic joints are usually controlled by a single symmetrical actuator, asymmetrical actuation may offer benefits for real-world tasks. To better understand optimal design of asymmetrical actuation, we present a model that integrates active and passive mechanical properties of a joint. To obtain general insights, we use a non-dimensional framework to simulate joint performance in different dynamical regimes. Our results show that incorporating joint passive elasticity effectively compensates for the imbalance between actuators when asymmetric actuation is utilised. These results highlight a novel contribution of active-passive interactions, offering valuable insight for the design of bioinspired robotic joints.

Keywords: Joint Dynamics · Muscle Asymmetry · Passive Mechanics · Non-dimensional Modelling · Bioinspired Robotics.

1 Introduction

Animal motor control seamlessly integrates dexterity, force, speed, and energy efficiency, capabilities that remain challenging to replicate in robotic systems. Despite the structural and functional conservation of muscles across species, from microscopic organisms to whales, replicating their performance in engineered systems has proven difficult. Although robotic actuators can mimic certain muscle properties and control strategies, many functional advantages arise from anatomical configurations. One such configuration, nearly universal in animals, is the use of antagonistic muscle pairs to control joints. This arrangement arises a fundamental limitation of biological muscles: active contraction is possible, but active lengthening is not. Muscles must return to their resting length

either through passive relaxation or by being stretched by forces of an opposing muscle. In contrast, since robotic actuators can generate opposing forces independently, antagonistic pairing has received limited attention.

Another key distinction between muscle-based and robotic actuators is actuator asymmetry, particularly in their force production capabilities, resulting in joints that apply torque asymmetrically in both directions. In biological systems, joints are often actuated by muscles with unequal strength: the agonist muscle is typically larger and more powerful, enabling it to generate the substantial forces required for load-bearing or gravity-resisting tasks. In contrast, the antagonist often provides fine control and joint stabilisation [28]. In biology, this asymmetry is seen as an evolved optimisation for efficient joint control in bodies performing varied tasks, which remains unexplored in robotics. We address this using a model that includes a muscle-like actuator pair to control a load-bearing joint.

The properties of a pair of muscles are highly optimised to achieve the desired joint control behaviour, but the passive elements significantly modulate this outcome. Within the joint system, elements such as tendons, ligaments, connective tissues, and other viscoelastic components interact dynamically with the agonist and antagonist muscle pair. These interactions influence the transmission of force, enable the storage and release of elastic energy, and ultimately shape the torque produced at the joint [2,3,4,9,17,19,32]. The integration of active and passive elements forms the basis of complex joint biomechanics, where the evolved asymmetry in active force generation and the mechanical properties of passive tissues together produce the diverse limb movements observed in animals.

Unlike biological joints, engineered robotic joints have largely adopted symmetric actuation. Robotic joints typically employ a single actuator to generate motion in both directions. Many designs adopt standardised gear ratios, motor properties, or identical actuator units, resulting in symmetric torque production [23]. Even in setups with two actuators, the two are often identical, yielding nearly equal torque output in opposing directions [8,10,18,30]. This design simplifies the assembly and control of robotic systems, but may not represent the most dexterous or energy-efficient approach. In addition, biological actuation presents inherent compliance. The importance of passive and active compliant mechanisms for efficiency and robustness has been noted for decades [5,13,20,31]. With the advent of robotic technologies, the incorporation of such passive elements has accelerated considerably over the last decade [1,11,16,25].

To better understand the benefits and limitations of bioinspired joint design, we ask whether strategies observed in biological systems, where muscle asymmetry and integrated passive structures work together, can offer more robust joint control than conventional symmetric actuation schemes. To address this question in a broadly applicable manner, we developed a non-dimensional framework to study joint dynamics and the relative effects of mechanical properties within the system. This approach focuses on key dimensionless variables, allowing comparison across systems of varying scales. Our framework elucidates the critical interaction between active and passive elements in both symmetrical and asym-

metrical actuator configurations, demonstrating how these factors collectively shape joint performance.

2 Methods

2.1 Framework Overview

We developed a compact mechanical model of a hinge joint with a single rotational degree-of-freedom (DoF, Fig. 1). Our model can be used for any single joint, but is inspired by a knee joint connecting the femur (proximal link) to the tibia (distal link). The focus on a single DoF provides fundamental insight while being generally applicable as most robotic systems are built from serially connected single-DoF joints in a wide range of different configurations.

In our model, two antagonistic muscle-tendon units (MTUs) called extensor and flexor rotate the distal link of the joint. The extensor MTU increases the joint angle, and the flexor MTU decreases it. These motions are also called extension and flexion, respectively. The motion of the joint is also subject to external load and the internal passive properties of the muscle-tendon units and joint. Hence, our model captures three hallmarks of biological joints: (i) pairs of asymmetric actuators, which are modelled as (ii) compliant Hill-like muscles [12] that control (iii) passive viscoelastic joints [28,31].

Our model collapses the complexity of muscles and tendons into a compact MTU with non-linear adaptive stiffness and viscosity, while the joint is minimally represented by linear stiffness and damping terms. In so doing, we retain sufficient fidelity to capture key qualitative features of joint dynamics while ensuring that the model remains manageable to obtain fundamental insights that are applicable to a variety of configurations.

2.2 Muscle-Tendon Unit Model

The system was designed with flexor and extensor muscle-tendon units, each modelled by a spring-damper system that is driven by a corresponding input activation signal A_m. Following the model and notation of Boyle et al. [6], each contractile element is a variable spring with dynamic coefficient κ_a, and a parallel dynamic damper with coefficient β_a (flexor inset Fig. 1A). The state-dependent modulation of actuator stiffness and damping coefficients is implemented as a simplified piece-wise linear approximation of the intrinsic force-length and force-velocity relationships described by Hill's muscle model [6,12].

For each muscle $i = \{\text{fl},\ \text{ext}\}$, the total active contractile force is given by:

$$F_i = \kappa_a^{(i)}(L_t^{(i)} - L_m^{(i)}) - \beta_a^{(i)}\dot{L}_m^{(i)}\,, \tag{1}$$

where L_m denotes the muscle length, the dot denotes time differentiation (hence $\dot{L}_m$ is the muscle contraction rate). For this study, the length of the flexor and

extensor MTUs are defined geometrically as $L_m^{\text{fl}} = -L_m^{\text{ext}} = -\cos\theta$. L_t denotes the activation-dependant tension length of the spring element, given by:

$$L_t^{(i)} = L_0^{(i)} - \sigma(A_m^{(i)})(L_0^{(i)} - L_{\min}^{(i)})\,,$$

where L_0 is the muscle resting length and $L_{\min}$ is the minimum muscle length during full activation. The dynamic stiffness κ_a and damping β_a are defined as:

$$\kappa_a^{(i)} = \kappa_{\max}^{(i)}\sigma(A_m^{(i)})F_{\max}^{(i)}\,,$$
$$\beta_a^{(i)} = \beta_{\max}^{(i)}\sigma(A_m^{(i)})F_{\max}^{(i)}\,,$$

where $\kappa_{\max}$, $\beta_{\max}$ and $F_{\max}$ are constants. The piece-wise linear function $\sigma(\cdot)$ clips the muscle activation signal A_m to the allowable range; it is defined as:

$$\sigma(y) = \begin{cases} 0: & y < 0 \\ y: & 0 < y < 1 \\ 1: & y > 1\,. \end{cases}$$

The adoption of Hill-like muscles allows us to combine viscoelasticity in the muscles and in the joint, as well as dynamic compliance in the muscles. Within the robotic context, Hill-like muscles capture interesting properties of pneumatic actuators [21], which are also of interest in systems employing antagonistic actuation pairs [8,10]. In addition, Hill-like actuation has been of interest for biorobotics [11,24,27] and may offer advantages in robotic applications such as exoskeletons that directly control the human body [15,29]. As our focus in this study will be on the costs and benefits of muscle and joint mechanical properties, we keep the electrical parameters of the Hill-like muscle model fixed.

2.3 Joint Model

To model the joint, we represent the distal link as a rigid rod of length l and mass m with uniform density. The proximal link is assumed to be fixed, providing a static anchor for the joint. We attach both links via a hinge joint, that is free to rotate about a single, fixed axis (blue circle Fig. 1A). At rest, the distal link hangs perpendicular to the proximal link, defining a joint angle of $\theta_{\text{rest}} = 90°$, which serves as our reference state for analysing the contributions of both active and passive forces. The extensor and flexor MTUs apply force to the distal link in a horizontal direction, from fixed attachment points relative to the joint. At θ_{rest}, their moment arms of length r_{ext} and r_{fl}, respectively, are perpendicular to the distal link. As the joint angle θ changes, the moment arms vary in length accordingly: $r_{\text{fl}} = -r_{\text{ext}} = \sin\theta$.

For compactness, we combine the passive properties of the different joint elements into two parameters: the passive elasticity, κ_p, and damping, β_p. These are modelled as a rotational spring-damper (circled inset Fig. 1). By treating the joint as a linear element, the non-linearity is subsumed into the muscle model.

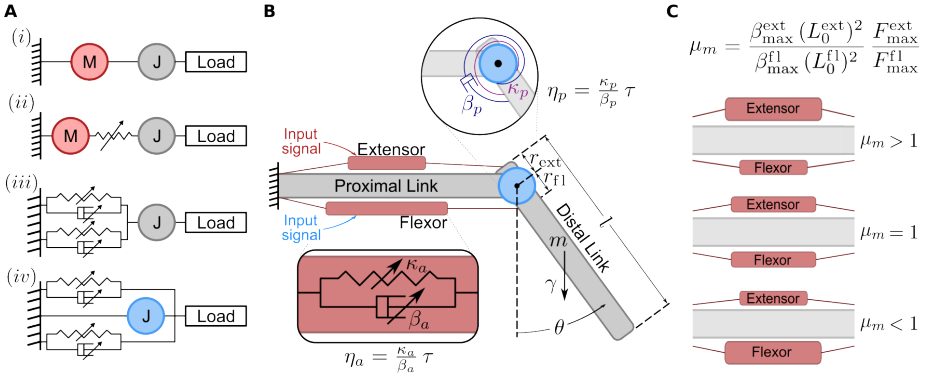

Fig. 1. (A) Actuation models for load-bearing joint. (*i*) Rigid motor, rigid joint (no passive elements) (*ii*) variable-stiffness actuator, rigid joint (*iii*) pair of antagonistic Hill-like actuators, rigid joint (*iv*) pair of antagonistic Hill-like actuators, viscoelastic joint (active and passive elements). **(B)** Schematic of the joint model (*iv*). At rest, the joint angle θ between the proximal and distal links is θ_{rest}, here set to 90° (without loss of generality). The distal link, with mass m, is connected to the proximal link via a rotational spring-damper system with passive stiffness κ_p and damping β_p. Flexor and extensor MTUs are positioned on either side of the proximal link, tethered to its free end and the near end of the distal link. Muscles are modelled as linear spring-damper elements with variable stiffness κ_a and damping β_a. Dimensionless parameters η_a and η_p capture the stiffness-to-damping ratio of the active muscles and passive joint, respectively. Load is represented by a gravity-like parameter γ. **(C)** The dimensionless parameter μ_m denotes the relative muscle force production of the extensor to the flexor.

The net torque on the joint results from the active muscle torques, the passive joint properties, and the weight of the distal link acting at its centre of mass:

$$T_{\mathrm{net}} = \sum_{i=\{\mathrm{fl},\,\mathrm{ext}\}} F_i\, r_i - \kappa_p\, \Delta\theta - \beta_p\, \dot{\theta} - \frac{mgl\sin\theta}{2}\,, \tag{2}$$

where $\Delta\theta = \theta - \theta_{\mathrm{rest}}$. Including the moment of inertia J of the distal link, the rotational equation of motion follows from $J\ddot{\theta} = T_{\mathrm{net}}$. Then, substituting the expression for T_{net} yields the complete equation governing joint motion:

$$\ddot{\theta} = \frac{1}{J}\left(\Sigma_{i=\{\mathrm{fl},\,\mathrm{ext}\}} F_i\, r_i - \kappa_p\, \Delta\theta - \beta_p\, \dot{\theta} - \frac{mgl\sin\theta}{2}\right). \tag{3}$$

2.4 Non-dimensionalisation

To non-dimensionalise the joint model, we normalise the muscle length L_m by the characteristic muscle length L_0 to obtain $L_m = L_0\,\hat{L}_m$, and the time t by the characteristic cycle period τ to give $t = \tau\,\hat{t}$. Here, $\hat{}$ denotes a dimensionless variable. As a behaviourally relevant timescale for animals and robots, the period

of one full joint cycle is chosen to be $\tau = 1\,s$. Substituting these definitions into Eq. (1) produces the dimensionless muscle force equation for both flexor and extensor (i):

$$\hat{F}_i = \eta_a^{(i)}(\hat{L}_t^{(i)} - \hat{L}_m^{(i)}) - \hat{\dot{L}}_m^{(i)}\,, \tag{4}$$

where

$$\eta_a^{(i)} = \frac{\kappa_{\max}^{(i)}}{\beta_{\max}^{(i)}}\,\tau\,.$$

Likewise, the substitution of the dimensionless variables into Eq. (2) results in the dimensionless net torque:

$$\hat{T}_{\text{net}} = \mu_j\,(\hat{F}_{\text{fl}}\,\hat{r}_{\text{fl}} + \mu_m(\hat{F}_{\text{ext}}\,\hat{r}_{\text{ext}})\,) - \eta_p(\Delta\theta) - \dot{\theta} - \gamma\,(\sin\theta)\,, \tag{5}$$

where

$$\mu_j = \frac{\Sigma_{i=\text{fl, ext}}\,\beta_{\max}^{(i)}\,F_{\max}^{(i)}\,(L_0^{(i)})^2}{\beta_p},$$

$$\mu_m = \frac{\beta_{\max}^{\text{ext}}\,(L_0^{\text{ext}})^2}{\beta_{\max}^{\text{fl}}\,(L_0^{\text{fl}})^2}\,\frac{F_{\max}^{\text{ext}}}{F_{\max}^{\text{fl}}}\,, \quad \eta_p = \frac{\kappa_p}{\beta_p}\,\tau, \quad \gamma = \frac{mgl}{2\beta_p}\,\tau\,.$$

Finally, including the scaled moment of inertia of the rod $\frac{J}{\beta_p\tau}\,\ddot{\theta} = \hat{T}_{\text{net}}$, yields the dimensionless equation of motion:

$$\hat{T}_{\text{net}} = \frac{1}{\hat{J}}\left[\mu_j(\hat{F}_{\text{fl}}\;\hat{r}_{\text{fl}} + \mu_m(\hat{F}_{\text{ext}}\;\hat{r}_{\text{ext}})) - \eta_p(\Delta\theta) - \dot{\theta} - \gamma\,(\sin\theta)\right]\,, \tag{6}$$

where the dimensionless moment of inertia is defined as:

$$\hat{J} = \frac{J}{\beta_p\tau}\,.$$

The non-dimensional formulation allows us to define a key set of parameters that encapsulate critical physical properties of the joint system. The parameters $\eta_a^{(\text{fl, ext})}$ and η_p represent the ratios between the stiffness and the damping of the active muscle-tendon units and the passive joint, respectively. They describe whether the joint system behaves more like an elastic spring or a viscous damper.

The dimensionless parameter μ_m quantifies the relative torque capacity of the extensor compared to the flexor (Fig. 1B). In other words, μ_m indicates how much the torque production of the extensor outweighs, or is outweighed by, that of the flexor. In the symmetric case ($\mu_m = 1$), both muscles contribute equally. The asymmetric regimes $\mu_m > 1$ (or $\mu_m < 1$) correspond to a stronger (or weaker) extensor. Similar to μ_m, μ_j measures the ratio of the active (muscle generated) to passive (joint generated) torques.

The gravitational torque, γ, is a specific example of a mechanical load. It denotes the ratio between the mechanical load, here the gravitational torque of the distal link, and the passive joint damping. For $\gamma \gg 1$, gravitational forces will have a dominant effect on joint motion, flexing or extending it, depending on the orientation of the distal link. Finally, the dimensionless moment of inertia $\hat{J}$ encapsulates the effect of the distal link's rotational inertia on the joint dynamics. High values of $\hat{J}$ correspond to a greater inertial effect.

3 Results

To establish baseline results for the non-dimensional framework, we evaluated passive joint dynamics without active actuation (Fig. 2). In these experiments, the distal link was initially deviated to an extended angle θ_{dev}, and then allowed to flex entirely passively to its resting state θ_{rest}. To characterise the relaxation dynamics, we define the relaxation time τ_{relax} as the time needed for the joint angle to decay to $1/e$ of its initial deviation. Note that identical behaviour is observed for passive relaxation due to flexion (Fig. 2) and extension (not shown).

The results show different behavioural regimes: when both the passive stiffness-to-damping ratio η_p and the dimensionless inertia $\hat{J}$ are low, the joint returns to equilibrium slowly and monotonically, with overdamped responses and relaxation dominated by damping (bottom-left corner in Fig 2B). By contrast, high values of η_p and $\hat{J}$ lead to underdamping and oscillatory settling (top-right corner in Fig 2B). This leads to faster transient responses but introduces challenges for stability and control. Moreover, under high gravitational load γ, a strong restoring torque accelerates the passive return to equilibrium. Whereas for low load, the response is primarily governed by elasticity and damping. Overall, higher η_p results in faster returns to rest. Consequently, when $\hat{J}$ is small the effect of inertia is negligible, and the relaxation time is nearly entirely governed by passive viscoelastic properties of the system.

A central question in our study is how active muscle actuation interacts with joint passive properties to determine its dynamic range and frequency response. While future work could explore metrics such as energy efficiency, force control precision, and robustness to disturbances, we focus here on the peak-to-peak amplitude θ_{p2p}, a basic observable and functionally relevant metric of joint performance during rhythmic motion. We first examined joint dynamics under symmetric muscle configuration, $\mu_m = 1$ (Fig. 3), where the distal link was driven by alternating sinusoidal activations of the flexor and extensor MTUs, producing periodic oscillations about the resting state θ_{rest}. The resulting joint motion was analysed as a function of the parameters η_a, η_p, and the activation frequency $\hat{f} \equiv 1/\hat{t}$. To visualise the results in 2D plots, we set $\gamma = 1$ and $\hat{J} = 0.1$.

Fig. 3B illustrates how active (η_a) and passive (η_p) components of the system shape the dynamic range of the joint, while Fig. 3C shows a similar interplay between η_a and the activation frequency $\hat{f}$. Notably, both cases reveal three distinct dynamic regimes. In regime I, either the passive stiffness is insufficient (panel B), or the activation frequency is sufficiently low (panel C), so that the dynamic range depends almost entirely on η_a. In other words, the active properties of the muscle directly determine the amplitude in this regime. In regime II, joint motion reflects a balance between η_a and η_p (panel B) or $\hat{f}$ (panel C), causing the contour lines to tilt diagonally. This indicates that maintaining large amplitudes requires increasing η_a proportionally alongside η_p (or $\hat{f}$). In the limit of high active stiffness and low passive damping, we recover the behaviour of an ideal rigid joint (Fig. 1A (i)). In regime III, where both the passive stiffness and the activation frequency are sufficiently high that the amplitude is nearly damped out. In this regime, the motion of the joint is almost static.

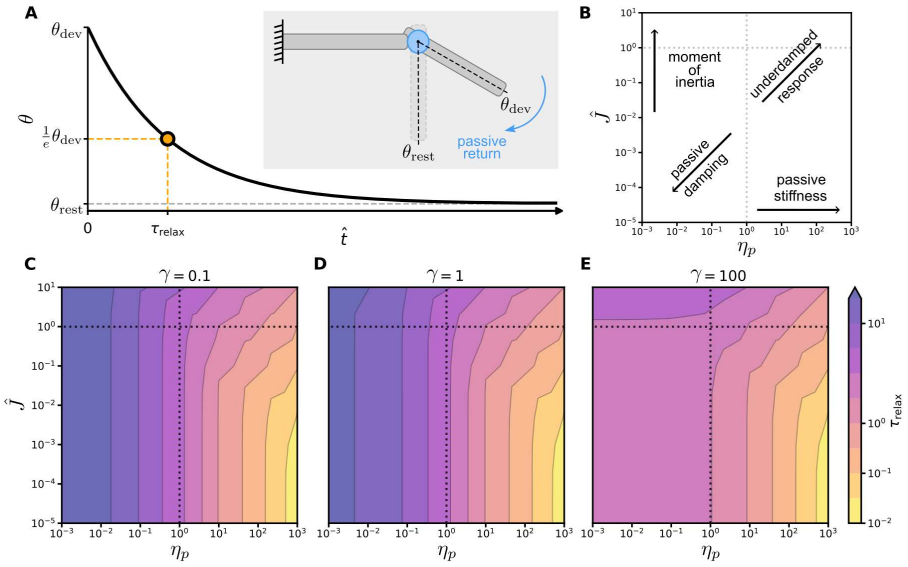

Fig. 2. Passive joint dynamics. **(A)** An overdamped relaxation trajectory of the joint angle $\theta(\hat{t})$. Orange marker denotes the time point at which the joint angle has decayed to θ_{dev}/e of its initial deviation. The inset indicates the distal link returning passively from the deviation angle θ_{dev} to the resting position θ_{rest}. **(B)** Schematic of the parameter space spanned by the passive stiffness-to-damping ratio η_p and the dimensionless moment of inertia $\hat{J}$. The upward arrow indicates increasing inertia, while the horizontal arrow denotes increasing passive stiffness. The lower-left region is dominated by passive damping, whereas the upper-right corner reflects an underdamped response. **(C-E)** Dimensionless relaxation time τ_{relax} as a function of the variables η_p and $\hat{J}$ for $\gamma = 0.1$, $\gamma = 1$, and $\gamma = 100$, respectively. Blue-tone colours indicate longer relaxation times (*i.e.*, slower returns), while yellow-tone colours denote faster convergence to the resting state. Dotted lines indicate where $\eta_p = 1$, and $\hat{J} = 1$.

The interaction between the passive properties of the joint η_p and the activation frequency $\hat{f}$ is illustrated in Fig. 3D. A black solid line separates two regimes. Below this line, the passive stiffness dominates. As η_p increases, the ability of the muscles to bend the joint is reduced. Hence, the range of motion of the joint diminishes. Above the line, higher frequencies are less effective at producing large joint displacements, leading to lower amplitudes. In regions where both η_p and $\hat{f}$ remain below 1, the amplitude is only weakly influenced by these parameters, relying primarily on the muscle's active properties. Conversely, when η_p and $\hat{f}$ exceed 1, maintaining a desired amplitude requires balancing the passive stiffness with the activation frequency.

In order to understand how muscle asymmetry influences joint dynamic range, we asked how the variations in muscle asymmetry μ_m influence the peak-to-peak amplitude of joint motion, and how this interplay interacts with the ac-

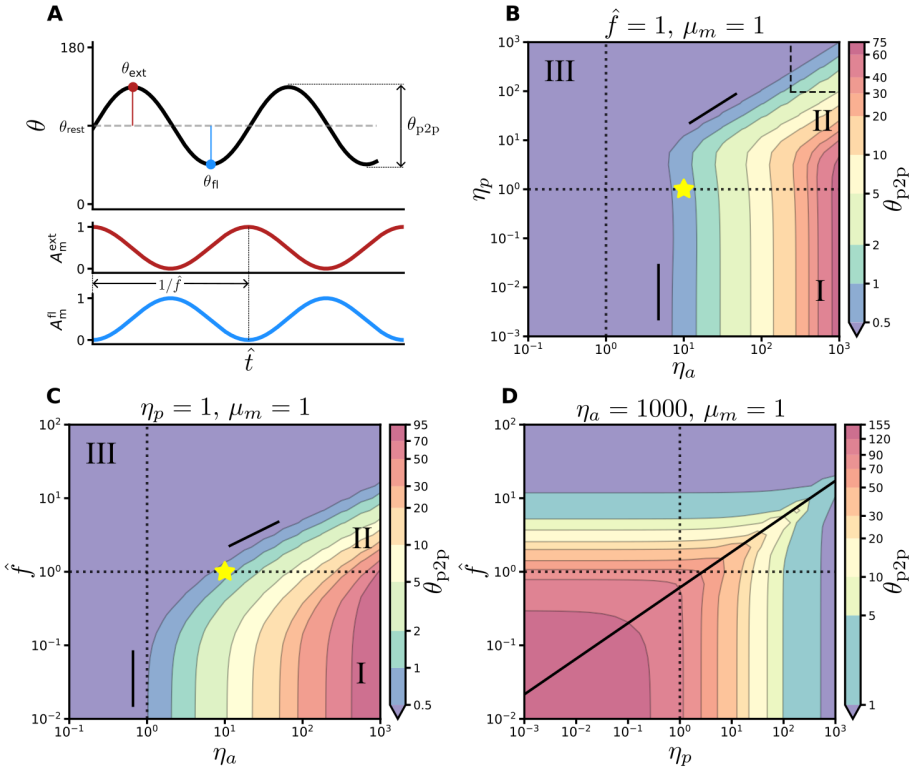

Fig. 3. Joint angle dynamics with symmetric muscle actuation. **(A)** Top: Joint angle $\theta(\hat{t})$. Bottom: Muscle activation $A_m^{(\text{ext, fl})}(\hat{t})$. Peak extension θ_{ext} (red) and flexion θ_{fl} (blue) are equal, showing symmetrical oscillations. The contour plots of the peak-to-peak joint angle amplitude θ_{p2p} as a function of dimensional variables including **(B)** η_a and η_p. Dashed box: high active stiffness and low passive damping parameter region approximating a rigid joint. **(C)** η_a and $\hat{f}$, and **(D)** η_p and $\hat{f}$. Panels B and C reveal similar dynamic regimes, numbered as I, II, and III. The point $\eta_a = 1000$, $\eta_p = 1$, and $\hat{f} = 1$ is represented with a yellow star. Warmer colours indicate larger amplitudes. Dotted lines indicate where $\eta_a = 1$, $\eta_p = 1$, and $\hat{f} = 1$. The remaining dimensionless variables are $\eta_a = \eta_a^{\text{fl}} = \eta_a^{\text{ext}}$, $\mu_j = 1$, $\gamma = 1$, and $\hat{J} = 0.1$.

tivation frequency $\hat{f}$, and the active and passive components of the joint η_p (see Fig. 4). We maintain a fixed total muscle active capacity defined as $\eta_a^{\text{eff}} = 1000$, where $\eta_a^{\text{eff}} = \eta_a(1 + \mu_m)\,/\,2$. This formulation ensures that regardless of the degree of asymmetry, the overall active contribution remains constant regardless of μ_m. Consequently, while $\mu_m = 1$ yields equal contributions from the extensor and flexor MTUs, deviations from symmetry redistribute this constant capacity between the two actuators, directly influencing the dynamic response of the joint.

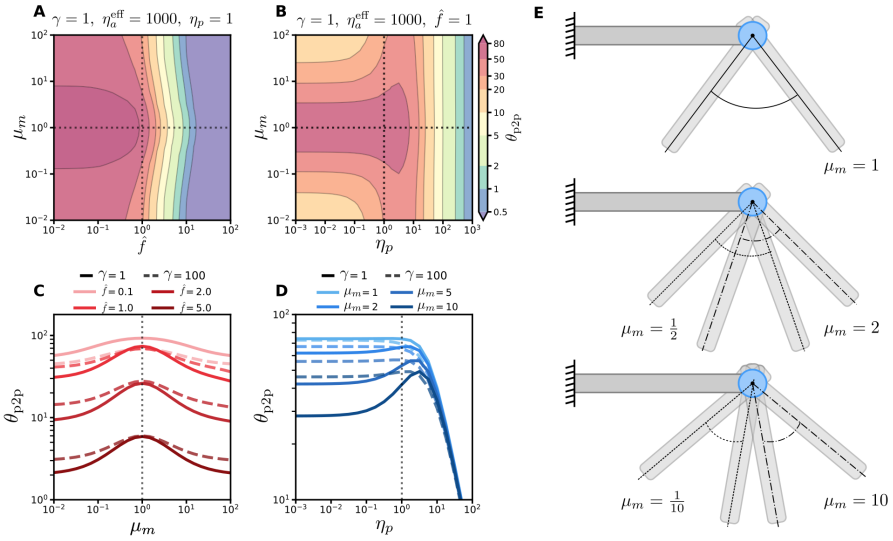

Fig. 4. Joint angle dynamics with asymmetric actuation. Peak-to-peak amplitude θ_{p2p} as a function of muscle asymmetry μ_m and **(A)** the activation frequency $\hat{f}$, and **(B)** the passive stiffness-to-damping ratio η_p, for a fixed $\gamma = 1$. Extracted line plots from panel B show θ_{p2p} as a function of **(C)** η_m for fixed values of $\hat{f}$, and **(D)** η_p for fixed values of μ_m. Solid and dashed lines correspond to $\gamma = 1$ and $\gamma = 100$, respectively. **E** Schematic representation of the joint's θ_{p2p} amplitude. From top to bottom: symmetric case ($\mu_m = 1$), with oscillation amplitudes evenly distributed about the rest angle. Two asymmetric configurations ($\mu_m = 2$, $\mu_m = 10$ and their respective inverse $1/\mu_m$), showing a biased dynamic range due to actuator imbalance.

As expected, our results (Fig. 4) show that muscle asymmetry shifts the dynamic range of the joint toward either extension ($\mu_m > 1$) or flexion ($\mu_m < 1$). However, the greater the asymmetry and resultant bias, the more limited the range of motion. Moreover, when the dynamics are muscle-dominated, reducing the activation frequency does not fully recover the dynamic range. Hence, naively, muscle asymmetry significantly limits the joint functionality. In contrast, while a low stiffness-to-damping ratio, η_p, appears preferable in the symmetric case, increasing passive joint stiffness in an asymmetrical configuration can mitigate these adverse effects. While the dynamic range remains slightly higher for the symmetric case, stiff joints (with $1 < \eta_p < 10$) maintain the directional bias whilst recovering nearly the full dynamic range. Furthermore, reduced frequencies now result in similarly increased peak-to-peak amplitudes to the symmetrical configuration. Hence, passive stiffness, arranged in parallel to the actuators (Fig. 2), stores and routes the energy within the system and thus provides robustness in the face of asymmetrical actuation.

This effect depends on joint loading. At low loads ($\gamma = 1$), moderate passive stiffness enhances symmetry breaking and supports a robust dynamic range

across a consistent η_p range, even with actuator asymmetry. At high loads ($\gamma = 100$), staying within this optimal η_p range becomes crucial to maintain motion. These findings highlight the need to optimise passive properties in asymmetrically actuated joints to reduce performance trade-offs.

4 Discussion

Biological joints are characterised by passive viscoelastic properties that play a crucial role in joint motion [3,4,22]. This effect is particularly pronounced in insects and small animals, where low inertia and minimal gravitational forces enhance the contribution of passive elements [2,14,26,32]. Although actuator compliance, where passive elements are arranged in series with actuators to mimic biological tendons, has been explored in robotics, designs incorporating passive viscoelastic elements in parallel remain relatively underutilised. The present model addresses this limitation by integrating both muscle compliance and joint-level passive viscoelasticity.

To investigate the joint dynamic regimes and associated timescales under symmetrical and asymmetrical conditions, we apply a fixed load, either low or high, and drive the actuators with a sinusoidal input. The response of the joint can be interpreted using a filter analogy. When muscle stiffness dominates, under low or moderate load and with limited passive contribution, the joint behaves as a pass-through filter (regime I, Fig. 3B). In this regime, motion amplitude is largely preserved, damping is minimal, and phase delay is governed by the actuator's elastic timescale. As passive stiffness increases beyond a critical threshold, motion becomes attenuated, resembling a low-pass filter (regime II). When passive stiffness dominates over active stiffness, oscillations are almost entirely suppressed, consistent with a stop-band filter (regime III; see also Fig. 3C). The filter analogy provides intuition about the characteristic timescale of the system, for which the joint achieves maximum amplitude. These findings, derived from a general non-dimensional framework, are applicable across a wide range of joint sizes and loading conditions. In fact, the filter analogy extends beyond joints. A similar approach has also been applied to undulatory motion in invertebrate swimmers [7], demonstrating the broader relevance of dimensionless analysis in active-passive systems.

Although symmetric actuation configurations yield optimal joint performance by aligning with regime I and maximising range of motion, introducing asymmetry can be beneficial in specific contexts. These include load-bearing tasks or design constraints involving limited actuator power, weight, space, or cost. In biological systems, resting metabolic cost is another relevant factor. One clear disadvantage of actuator imbalance is its effect on dynamic range, shifting it toward either extension or flexion (Fig. 4E), and suppressing it. Symmetric configurations consistently outperform sufficiently asymmetric ones, regardless of actuation frequency.

We show that in tasks with directional bias (*i.e.*, unidirectional movement), passive joint compliance can mitigate against the imbalance and reduced dy-

namic range that occur due to muscle asymmetry (Fig. 4B). Under low-load conditions, when the passive stiffness-to-damping ratio exceeds unity, typically between one and ten, the joint reaches peak amplitude, indicating an optimal range that minimises attenuation. In symmetric configurations, any degree of passive stiffness attenuates the dynamic range. In asymmetric cases, performance improves significantly when passive properties are tuned within this optimal range (Fig. 4D). Even under high loads, effective joint motion can be maintained if passive stiffness remains close to its optimal value.

In conclusion, this study has demonstrated the usefulness of passive compliance in asymmetric biological or engineered systems, highlighting potential advantages as well as the inherent trade-offs of such asymmetric configurations. In symmetric configurations, passive joints did not provide a clear advantage, whereas in systems with asymmetrical actuation, their integration improved performance. These findings contribute to a broader understanding of joint mechanics across scales, with potential to inform the design of bioinspired robotic systems. Furthermore, the findings presented illustrate the usefulness of computational modelling for active-passive systems. Further extensions of the model framework presented here can be used to develop more sophisticated biomechanical and robotic systems that effectively balance structural constraints with functional demands.

This paper considered motion for a fixed configuration of the joint relative to the load. In addition, animals and robotic systems often move or alter their orientation to exploit the stronger actuator. By strategically incorporating higher dimensional control strategies alongside optimised passive properties, future robotic designs can better exploit actuator asymmetry to combine strength and dexterity. Such an approach must consider the configuration of the joints within larger bodies or robotic systems.

Discourse on joint dynamics often regards passive elements in isolation, rather than in the context of joint or system configuration. This paper revisits material properties in asymmetrically configured joint systems. The results presented here reinforce the necessity for a nuanced, context-aware approach to biomechanical engineering. Our motivation was both to deepen our understanding of biological movement and to serve as guiding principles for the next generation of robotics and biomechanical innovation. As robotic systems continue to evolve, leveraging asymmetry in conjunction with adaptive control and passive properties can help facilitate optimal performance across a range of applications, from prosthetics and assistive technologies to autonomous robotic platforms.

Acknowledgments. The authors thank Dr. Lukas Deutz, whose work inspired the interpretation of some of the results presented here. ERR acknowledges the financial support provided by the SECIHTI (grant no. 766606). NC thanks the EPSRC (EP/S016813/1, EP/S01540X/1) and ISPF (BB/Z514317/1) for support.

Disclosure of Interests. The authors have no competing interests to declare that are relevant to the content of this article.

References

1. Abadía, I., Bruel, A., Courtine, G., Ijspeert, A.J., Ros, E., Luque, N.R.: A neuromechanics solution for adjustable robot compliance and accuracy. Science Robotics **10**(98) (2025). https://doi.org/10.1126/scirobotics.adp2356
2. Ache, J.M., Matheson, T.: Passive joint forces are tuned to limb use in insects and drive movements without motor activity. Current Biology **23**(15), 1418–1426 (2013). https://doi.org/10.1016/j.cub.2013.06.024
3. Alexander, R.M.: Energy-Saving Mechanisms in Walking and Running. Journal of Experimental Biology **160**(1), 55–69 (1991). https://doi.org/10.1242/JEB.160.1.55
4. Alexander, R.M., Bennet-Clark, H.C.: Storage of elastic strain energy in muscle and other tissues. Nature **265**(5590), 114–117 (1977). https://doi.org/10.1038/265114a0
5. Bigge, B., Harvey, I.R.: Programmable springs: Developing actuators with programmable compliance for autonomous robots. Robotics and Autonomous Systems **55**(9), 728–734 (2007). https://doi.org/10.1016/J.ROBOT.2007.05.013
6. Boyle, J.H., Berri, S., Cohen, N.: Gait modulation in C. elegans: An integrated neuromechanical model. Frontiers in Computational Neuroscience **6**(10), 17123 (2012). https://doi.org/10.3389/fncom.2012.00010
7. Deutz, L.: Gait Modulation of Undulatory Microswimmers through the Lens of Optimality. Ph.D. thesis, University of Leeds (2024)
8. Dirven, S., McDaid, A.: A systematic design strategy for antagonistic joints actuated by artificial muscles. IEEE/ASME Transactions on Mechatronics **22**(6), 2524–2531 (12 2017). https://doi.org/10.1109/TMECH.2017.2766637
9. Dudek, D.M., Full, R.J.: Passive mechanical properties of legs from running insects. Journal of Experimental Biology **209**(8), 1502–1515 (2006). https://doi.org/10.1242/JEB.02146
10. Fujita, T., Shimoda, Y., Machida, K., Okui, M., Nishihama, R., Nakamura, T.: Development of Variable Viscoelastic Joint Module Performance Evaluation and Proposal of Application Examples. Actuators **11**(3), 89 (2022). https://doi.org/10.3390/act11030089
11. Goldsmith, C.A., Szczecinski, N.S., Quinn, R.D.: Neurodynamic modeling of the fruit fly Drosophila melanogaster. Bioinspiration & Biomimetics **15**(6), 065003 (2020). https://doi.org/10.1088/1748-3190/ab9e52
12. Hill, A.V.: The heat of shortening and the dynamic constants of muscle. Proceedings of the Royal Society of London. Series B - Biological Sciences **126**(843), 136–195 (1938). https://doi.org/10.1098/rspb.1938.0050
13. Hoffmann, M., Simanek, J.: The Merits of Passive Compliant Joints in Legged Locomotion: Fast Learning, Superior Energy Efficiency and Versatile Sensing in a Quadruped Robot. Journal of Bionic Engineering **14**(1), 1–14 (2017). https://doi.org/10.1016/S1672-6529(16)60374-8
14. Hooper, S.L., Guschlbauer, C., Blümel, M., Rosenbaum, P., Gruhn, M., Akay, T., Büschges, A.: Neural Control of Unloaded Leg Posture and of Leg Swing in Stick Insect, Cockroach, and Mouse Differs from That in Larger Animals. Journal of Neuroscience **29**(13), 4109–4119 (2009). https://doi.org/10.1523/JNEUROSCI.5510-08.2009
15. Hu, B., Zhang, F., Lu, H., Zou, H., Yang, J., Yu, H.: Design and Assist-as-Needed Control of Flexible Elbow Exoskeleton Actuated by Nonlinear Series Elastic Cable Driven Mechanism. Actuators **10**(11), 290 (2021). https://doi.org/10.3390/act10110290

16. Kwak, B., Lee, D., Bae, J.: Comprehensive analysis of efficient swimming using articulated legs fringed with flexible appendages inspired by a water beetle. Bioinspiration & Biomimetics **14**(6), 066003 (2019). https://doi.org/10.1088/1748-3190/ab36c0
17. Mcgeer, T.: Passive Dynamic Walking. The International Journal of Robotics Research **9**(2), 62–82 (1990). https://doi.org/10.1177/027836499000900206
18. Moore, R., Schimmels, J.M.: Design of a quadratic, antagonistic, cable-driven, variable stiffness actuator. Journal of Mechanisms and Robotics **13**(3) (2021). https://doi.org/10.1115/1.4050104/1098092
19. Patek, S.N., Dudek, D.M., Rosario, M.V.: From bouncy legs to poisoned arrows: Elastic movements in invertebrates. Journal of Experimental Biology **214**(12), 1973–1980 (2011). https://doi.org/10.1242/JEB.038596
20. Pratt, G.A., Williamson, M.M.: Series elastic actuators. IEEE International Conference on Intelligent Robots and Systems **1**, 399–406 (1995). https://doi.org/10.1109/IROS.1995.525827
21. Repperger, D.W., Phillips, C.A., Neidhard-Doll, A., Reynolds, D.B., Berlin, J.: Actuator design using biomimicry methods and a pneumatic muscle system. Control Engineering Practice **14**(9), 999–1009 (2006). https://doi.org/10.1016/j.conengprac.2005.06.009
22. Riener, R., Edrich, T.: Identification of passive elastic joint moments in the lower extremities. Journal of Biomechanics **32**(5), 539–544 (1999). https://doi.org/10.1016/S0021-9290(99)00009-3
23. Sakagami, Y., Watanabe, R., Aoyama, C., Matsunaga, S., Higaki, N., Fujimura, K.: The intelligent ASIMO: System overview and integration. IEEE International Conference on Intelligent Robots and Systems **3**, 2478–2483 (2002). https://doi.org/10.1109/IRDS.2002.1041641
24. Shen, X., Wang, X., Tian, M., Zhang, Q.: Modeling and sensorless force control of novel tendon-sheath artificial muscle based on hill muscle model. Mechatronics **62**, 102243 (2019). https://doi.org/10.1016/j.mechatronics.2019.06.003
25. Spenko, M.J., Haynes, G.C., Saunders, J.A., Cutkosky, M.R., Rizzi, A.A., Full, R.J., Koditschek, D.E.: Biologically inspired climbing with a hexapedal robot. Journal of Field Robotics **25**(4-5), 223–242 (2008). https://doi.org/10.1002/ROB.20238
26. Sutton, G.P., Szczecinski, N.S., Quinn, R.D., Chiel, H.J.: Phase shift between joint rotation and actuation reflects dominant forces and predicts muscle activation patterns. PNAS Nexus **2**(10) (2023). https://doi.org/10.1093/pnasnexus/pgad298
27. Szczecinski, N.S., Goldsmith, C.A., Young, F.R., Quinn, R.D.: Tuning a Robot Servomotor to Exhibit Muscle-Like Dynamics. In: Martinez-Hernandez, U., et al. Biomimetic and Biohybrid Systems. Living Machines 2019. Lecture Notes in Computer Science() **11556**, 254–265 (2019). https://doi.org/10.1007/978-3-030-24741-6{_}22
28. Wang, R., Yan, S., Schlippe, M., Tarassova, O., Pennati, G.V., Lindberg, F., Körting, C., Destro, A., Yang, L., Shi, B., Arndt, A.: Passive Mechanical Properties of Human Medial Gastrocnemius and Soleus Musculotendinous Unit. BioMed Research International **2021**, 8899699 (2021). https://doi.org/10.1155/2021/8899699
29. Wang, T., Zheng, T., Zhao, S., Sui, D., Zhao, J., Zhu, Y.: Design and Control of a Series–Parallel Elastic Actuator for a Weight-Bearing Exoskeleton Robot. Sensors **22**(3), 1055 (2022). https://doi.org/10.3390/S22031055

30. Yang, H., Wei, G., Ren, L., Yan, L., Caldwell, D.: Compliant actuators that mimic biological muscle performance with applications in a highly biomimetic robotic arm. Advanced Bionics **1**(1), 2–18 (2025). https://doi.org/10.1016/j.abs.2024.12.001
31. Zajac, F.E.: Muscle and tendon: properties, models, scaling, and application to biomechanics and motor control. Critical Reviews in Biomedical Engineering **17**(4), 359–411 (1989)
32. Zakotnik, J., Matheson, T., Dürr, V.: Co-contraction and passive forces facilitate load compensation of aimed limb movements. Journal of Neuroscience **26**(19), 4995–5007 (2006). https://doi.org/10.1523/JNEUROSCI.0161-06.2006